Biomicrofluidics ARTICLE scitation.org/journal/bmf

A microfluidic mammary gland coculture model using parallel 3D lumens for studying epithelial-endothelial migration in breast cancer

Cite as: Biomicrofluidics 13, 064122 (2019); doi: 10.1063/1.5123912
Submitted: 13 August 2019 · Accepted: 6 November 2019 ·
Published Online: 5 December 2019

Deepika Devadas,[1] Thomas A. Moore,[1] Noosheen Walji,[1,2] and Edmond W. K. Young[1,2,a)]

AFFILIATIONS

[1]Department of Mechanical & Industrial Engineering, University of Toronto, Toronto, Ontario M5S 3G8, Canada
[2]Institute of Biomaterials & Biomedical Engineering, University of Toronto, Toronto, Ontario M5S 3G9, Canada

[a)]**Author to whom correspondence should be addressed:** eyoung@mie.utoronto.ca. **Tel.:** +1 (416) 978-1521.

ABSTRACT

In breast cancer development, crosstalk between mammary epithelial cells and neighboring vascular endothelial cells is critical to understanding tumor progression and metastasis, but the mechanisms of this dynamic interplay are not fully understood. Current cell culture platforms do not accurately recapitulate the 3D luminal architecture of mammary gland elements. Here, we present the development of an accessible and scalable microfluidic coculture system that incorporates two parallel 3D luminal structures that mimic vascular endothelial and mammary epithelial cell layers, respectively. This parallel 3D lumen configuration allows investigation of endothelial-epithelial crosstalk and its effects of the comigration of endothelial and epithelial cells into microscale migration ports located between the parallel lumens. We describe the development and application of our platform, demonstrate generation of 3D luminal cell layers for endothelial cells and three different breast cancer cell lines, and quantify their migration profiles based on number of migrated cells, area coverage by migrated cells, and distance traveled by individual migrating cells into the migration ports. Our system enables analysis at the single-cell level, allows simultaneous monitoring of endothelial and epithelial cell migration within a 3D extracellular matrix, and has potential for applications in basic research on cellular crosstalk as well as drug development.

INTRODUCTION

The progression of breast cancer is a complex pathophysiological process that advances through a sequence of defined stages, from an overgrowth of epithelial cells lining the mammary ducts (epithelial hyperplasia) to the emergence of a noninvasive lesion known as ductal carcinoma *in situ* (DCIS) and eventually transitioning to invasive ductal carcinoma (IDC).[1] Subsequent invasion of tumor cells into the neighboring stroma sets the path toward intravasation into the bloodstream leading to metastasis.[2] Throughout this process, epithelial tumor cells interact with key elements of the mammary gland microenvironment, including other prominent cell types and the extracellular matrix (ECM), with many of the underlying mechanisms regulating these interactions still largely unknown.[3]

One critical interaction is the crosstalk between the mammary epithelial cells and the endothelial cells of nearby blood vessels. The vasculature exists to provide blood supply to the mammary gland,[4] and during tumor development, epithelial tumor cells migrate toward the vasculature and undergo endothelial transmigration to initiate the metastatic cascade.[2] Concurrently, angiogenesis may be occurring from the vasculature toward the developing tumour[5] and may be present even during the premalignant stage, as a result of increasing concentrations of vascular endothelial growth factor (VEGF) and other factors.[6] The dynamic interplay between epithelial and endothelial cells is complex and not well understood, especially in the presence of the other cell types and the ECM within the 3D mammary gland microenvironment. Understanding these interactions and the coordinated behaviors of endothelial and epithelial cells is critical to resolving the mechanisms of breast cancer progression and metastasis and may lead to the development of new therapeutic strategies that target angiogenesis and cell migration pathways.

To advance our fundamental understanding of these interactions, improved experimental models are necessary to better

mimic the physiological behavior of the cells within their tissue microenvironments.[7,8] Many researchers still rely on basic 2D cultures in well plates, Transwell membrane inserts and Boyden chambers to study cell migration, tumor cell invasion, and aspects of epithelial tumor-endothelial (TC-EC) cell signaling.[9–11] Other basic 2D cell-based assays (e.g., migration, invasion, and tubule formation assays) are commonly used to study angiogenesis.[12] However, the importance of capturing cell behavior and function in three dimensions has been well documented[13–15] and thus has led to the continued interest in the development of 3D organotypic models, including those that specifically model vascular endothelial-breast epithelial interactions in 3D coculture.[16]

In recent years, microfluidic cell culture systems have emerged as useful experimental models to study various tumor-stromal interactions, and, more specifically, the interactions between tumor and endothelial cells. Engineered microfluidic systems have the advantage of allowing spatiotemporal control of various biotransport phenomena within microfabricated geometries, which enables the precise modeling of dynamic cell behavior within controlled microenvironments.[17,18] In terms of tumor-endothelial (TC-EC) interactions in particular, various microfluidic systems have been designed to investigate specific aspects of their coordinated behavior. Zheng *et al.* developed an automated valve-based microfluidic device that initially kept human umbilical cord endothelial cells (HUVECs) and HeLa cells (a cervical cancer cell line) separated by pneumatically controlled valves, which were later opened to allow tumor-endothelial crosstalk and concurrent migration of cellular fronts.[19] Zervantonakis *et al.* developed a microfluidic system to examine tumor cell intravasation across an endothelial barrier.[20] Huang *et al.* developed a microfluidic device to study tumor cell extravasation that combined shear flow effects on the vascular endothelium and the presence of whole blood.[21] In terms of angiogenesis, numerous microfluidic systems have also been developed to study different processes and conditions, from shear flow effects on vessel sprouting dynamics and anastomosis,[22,23] to the complex interactions between endothelial cells, fibroblasts, and macrophages.[24] These examples represent only a small subset of the many microfluidic devices reported to date for studying vascular biology, tumor-endothelial interactions, cell migration, and angiogenesis, and many thorough reviews about these technological advancements are available for interested readers.[18,25–28]

Despite these advances, many aspects of the 3D microenvironment of the mammary gland remain underdeveloped or unexplored. In the examples above, migrating cellular fronts were examined on 2D flat surfaces of the floor of the microchannels,[19] neglecting important aspects of 3D cell migration in surrounding ECM.[29] Tumor-endothelial models that study intravasation and extravasation have focused on creating the luminal structure of the endothelium, but were not intended to capture the luminal structure of the mammary ducts.[20,21] Bischel and co-workers have previously demonstrated the use of 3D lumens to independently study endothelial-stromal interactions in angiogenesis,[30] as well as to model epithelial-fibroblast interactions in a DCIS microenvironment.[31] Lee and co-workers used 3D bioprinting to achieve large ~1-mm diameter lumens to create parallel vascular channels.[32] However, to date, an *in vitro* model that incorporates both vascular endothelial and mammary epithelial layers as 3D luminal structures has not been demonstrated, and furthermore has yet to be applied to study epithelial migration or premalignant angiogenesis.

Here, we present the development of an accessible 3D microfluidic model that incorporates two parallel 3D luminal structures for mimicking the vascular endothelial and mammary epithelial layers, respectively. Device design, microfabrication, and matrix and cell loading procedures are described, and imaging results and analyses are discussed to offer insight into the concomitant migration of epithelial and endothelial cells in this coculture model. Notably, three different breast cancer cell lines were chosen for the model to represent noncancerous (MCF-10A), noninvasive (MCF-7), and highly metastatic (MDA-MB-231) epithelial cell types. Our method enables analysis at the single-cell level and allows simultaneous monitoring of endothelial and epithelial cell migration within a 3D ECM, revealing different trends in matrix-dependent migratory behavior between cell phenotypes.

MATERIALS AND METHODS

Microfluidic device design and fabrication

Our device consisted of a 2×2 array of microfluidic culture systems [Fig. 1(a)], with each culture system designed to include two parallel long microchannels (500-μm wide $\times$ 350-μm tall $\times$ 7-mm long from inlet to outlet port) connected by three interconnecting conduits (i.e., migration ports, 320-μm wide $\times$ 100-μm tall $\times$ 720-μm long) [Fig. 1(b)]. The two parallel long microchannels were designed for the parallel lumens to mimic the 3D structure of an endothelial lumen and epithelial lumen, respectively. The geometry allowed a hydrogel mixture to be introduced through the open access ports, fill the entire channel network, and then remain pinned within the migration ports during lumen generation when most of the hydrogel in the main microchannels was removed [Fig. 1(c)]. The migration ports were sized to facilitate the formation of chemokine gradients along the length of the migration port and to enable visualization of cell migration from one microchannel to the other. Inlets and outlets for these channels allowed separate access to the channels and were sized to allow fluidic exchange via passive pumping.[33] We fabricated an additional media reservoir layer with a ~40-μl volume capacity per well above an inlet or outlet and bonded this layer to the channel layer. The reservoirs reduced the frequency of medium exchanges (once per 24-h) while improving cell viability and stability of the culture in the microchannels for longer times. Our group recently developed theoretical and computational models of angiogenesis in microfluidic channels specifically for this microfluidic device design.[34] This modeling was useful for guiding the design of different geometric features, such as the length and width of migration ports.

Devices were fabricated by conventional soft lithography.[35] Briefly, a complete SU-8 master mold with microchannel and port features was fabricated in a cleanroom facility using photolithography techniques, as previously described.[36] Poly(dimethylsiloxane) (PDMS) with a 10:1 (w/w) ratio of elastomer base to a curing agent was mixed, vacuum-desiccated to remove bubbles, and then poured on the master mold. The PDMS and master mold were placed on a hot plate to cure the PDMS at 80 °C for 4 h. PDMS layers with ports and channels were then bonded to $1'' \times 3''$ glass slides using oxygen plasma treatment. Glass was used as the underlying substrate to facilitate standard phase contrast and fluorescence

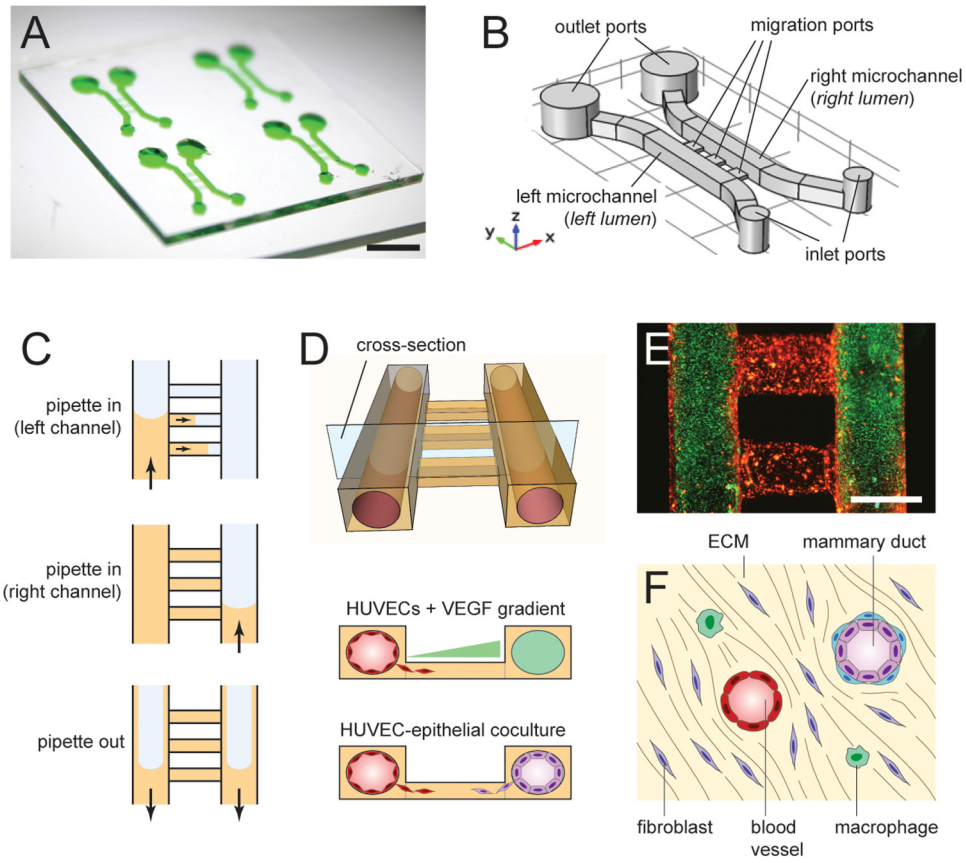

FIG. 1. Parallel 3D lumens. (a) Array of parallel 3D lumen microfluidic culture systems on a glass slide (scale bar = 5 mm). (b) Design of a parallel lumen microfluidic system, showing left and right microchannels, connected by three parallel migration ports. (c) Procedure for generating lumens involves: (i) filling an empty system with prepolymerized hydrogel solution starting with the left microchannel and allowing the gel to fill the migration ports and pin at the openings to the right microchannel; (ii) filling the right microchannel to connect the gel; and (iii) pipetting the gel out of the channels leaving a thin gel that coats the inner wall of the microchannels. (d) 3D model of parallel lumens. Cross sections show two experimental setups: (i) chemotaxis of endothelial cells and (ii) comigration of endothelial and epithelial cells. (e) Fluorescent microbeads representing the hydrogel (red beads) and the lumens (green beads). Scale bar = 500 μm. (f) Normal mammary gland microenvironment with various cell types and neighboring blood vessel and mammary duct luminal structures.

microscopy. Media reservoir PDMS layers were similarly bonded to the surface of the main PDMS layer to create the final device.

Cell culture

HUVECs were sourced from Lonza (CC-2519, Lonza; purchased from Cedarlane Labs, Burlington, ON, Canada). Cells were routinely cultured in T-25 flasks at the recommended concentration of 2500 cells/cm^2 at 37 °C and 5% CO_2 in EGM BulletKit medium (CC-3124, Lonza) for up to 7 passages. Note that EGM BulletKit was chosen because it does not contain any exogenous VEGF in its medium composition. The mammary epithelial cell lines MCF-10A, MCF-7, and MDA-MB-231 were sourced from ATCC (purchased from Cedarlane Labs). MCF-10A cells were cultured in Dulbecco's Modified Eagle Medium (DMEM)/F-12 media (Thermo Scientific) containing 5% horse serum (Sigma-Aldrich), 20 ng/ml epidermal growth factor (EGF; Sigma), 10 μg/ml human insulin (Sigma), and 500 ng/ml hydrocortisone (Sigma). MCF-7 and MDA-MB-231 cells were cultured in DMEM media containing 10% fetal bovine serum (FBS).

Lumen generation

Microfluidic systems were rinsed with 3 successive volume replacements (VRs) of 70% ethanol followed by 3 successive VRs of phosphate-buffered saline (PBS). Microfluidic systems were then incubated with 100 μg/ml of fibronectin (F1141, Sigma-Aldrich) for 20 min at room temperature. To generate cylindrical lumens in the two main microchannels, we used a modified version of the viscous finger patterning technique.[30] A cold hydrogel mixture of 20% growth-factor-reduced Matrigel (~10 mg/ml stock, #354230, Corning) and ~5.5 mg/ml of rat-tail Type-I Collagen (#354249, Corning) was introduced into precooled channels and migration ports and incubated for 3 min at 37 °C. The hydrogel mixture first filled one microchannel and then flowed into the three migration ports, pinning at the edge of the second microchannel [Fig. 1(c)]. This hydrogel pinning effect has also been demonstrated by others.[37,38] Prepolymerized hydrogel was then gently aspirated leaving behind a coating of partially polymerized hydrogel on the channel walls in the shape of a cylindrical lumen [Fig. 1(c)]. After further polymerization of at least 20 min at 37 °C, lumens were ready to be seeded.

Cell loading and assay setup

Prior to loading cells into microchannels, cells were labeled with CellTracker Green (#C2925, ThermoFisher) or CellTracker Red (#C34552, ThermoFisher) to distinguish between migrating cell types in coculture. All cell types were seeded into lumens at a concentration of ~24×10^3 cells per channel via passive pumping.

Devices were placed upside down and right side up for 15 min each to ensure uniform seeding along lumen walls, ceiling, and floor. Breast cancer migration assays were evaluated at 24 h postseeding after fixation with 4% formaldehyde. For endothelial cell migration assays, cells were serum-starved 24 h after seeding, in medium without FBS. VEGF was added at this step and cells were incubated for an additional 24 h before fixing and imaging. Images were obtained by fluorescence microscopy (EVOS FL Auto, Thermo Scientific) using a 10× objective at the site of each migration port.

Lumen microscopy and 3D reconstruction

Confocal images were obtained with a Plan Apo 10× objective mounted on a Nikon A1R confocal microscope and set at a 5-μm step size from the microchannel floor to the top of the lumen. Images were then reconstructed into 3D volumes using NIS Elements Software (Version 4.2).

Cell viability

Cell viability in lumens was assessed at 48 h postseeding using the LIVE/DEAD Viability/Cytotoxicity Kit for mammalian cells (L3224, ThermoFisher Scientific). After washing cells with PBS, cells were incubated with calcein AM (2 μM) and ethidium homodimer-1 (4 μM) in Opti-MEM reduced serum media (ThermoFisher Scientific) for 30 min at room temperature before washing with PBS. Devices were imaged using a fluorescence microscope (EVOS FL Auto, ThermoFisher Scientific) at 10× where live cells were stained green, dead cells were stained red, and nuclei were stained with Hoechst 33342 (ThermoFisher Scientific). Cell viability was expressed as the fraction of live cells in the population.

Cell migration metrics

Fluorescence images were analyzed using ImageJ, and three metrics were obtained: (i) number of migrated cells in a migration port, (ii) area covered by migrated cells in the migration port, and (iii) distances traveled by individual migrating cells. Each migration port region between the two lumen edges was considered a single independent region of interest (ROI). For the number of migrated cells in an ROI, cells were counted using the Find Maxima function with manual thresholding. For the area covered by migrated cells, images were first converted to 8-bit files, and then the area was determined using the Analyze Particles function (with a specified minimum cell size of 30 pixels). For distance traveled by individual migrating cells, cells identified by the Find Maxima function were located by listing their x-y coordinates, and then the x-coordinate for each cell was used to determine the (horizontal) distance traveled from the lumen edge. The combination of these three metrics constituted the overall "migration profile" of a particular cell type for a given experimental condition.

Statistical analysis

Each data point represented a single migration port in reference to cell counts and area metrics, while each data point represented a single cell for distance traveled. Red bars in each graph represented averages with standard errors of the mean. Data sets were statistically analyzed by analysis of variance (ANOVA) followed by Tukey's posthoc procedure to determine which conditions were significantly different.

RESULTS

Parallel 3D lumens

Both blood vessels and mammary ducts have luminal structures by nature and recapitulating this 3D architecture *in vitro* is important for establishing a representative tissue model that more accurately mimics physiological behavior of the mammary gland. Using our microfluidic culture system, and a lumen generation technique modified from Bischel *et al.*,[30] we created a mammary gland coculture model consisting of parallel 3D lumens [Fig. 1(c)], one lumen representing an endothelial-lined vessel, and the other representing an epithelial-lined duct. Our hydrogel and cell loading methods enabled confluent monolayers of endothelial and epithelial cells to coat their respective lumens at 24 h after seeding [Fig. 2(a)]. Luminal structures of the monolayers were verified by confocal microscopy, revealing rounded corners in the cross-sectional shapes, and clear images of the top and bottom cell layers of the lumens. Luminal structures were verified for all cell types used [MCF-10A, MCF-7, MDA-MB-231, HUVECs; Fig. 2(a) shows MCF-10A and HUVECs as representative]. Furthermore, cell-cell contacts within the HUVEC monolayers were confirmed by staining of CD-31 [Fig. 2(a)].

Cell viability in lumens

Cells in microfluidic channels consume nutrients and accumulate waste products more rapidly than cells in traditional macroscale platforms due to a much higher surface area-to-volume ratio.[17] In addition, because cells in a 3D cylindrical lumen have a further 3- to 4-fold increase in cell density compared to cells cultured in 2D, this issue of nutrient consumption and waste accumulation is further exacerbated in our lumen model. To ensure the viability of our model, we added a media reservoir of ~40-μl volume capacity above the outlet ports, and monitored cell viability of all cell types after 48 h, which was the maximum duration of our experiments. Cell viability for all cell types was found to be >85% [Figs. 2(b) and 2(c)], indicating that the coculture model can be successfully maintained for our experiments without the need for more frequent medium exchanges.

Cell migration between parallel lumens

We created parallel lumens with different cell combinations, using HUVECs containing CellTracker Red dye for the endothelial lumen (Fig. 3, left lumen), and one of the mammary epithelial cell lines containing CellTracker Green dye for the epithelial lumen (Fig. 3, right lumen). MCF-10A was chosen to model a normal mammary duct, while MCF-7 and MDA-MB-231 cell lines were chosen to model noninvasive and metastatic tumor epithelial cells of the breast, respectively. We anticipated differential migration behaviors of these cell lines into the migration port due to their inherent phenotypic differences. We also anticipated potential differential migration behaviors of HUVECs in the presence of these cell lines because each cell line represented distinct mammary microenvironments producing unique secretion profiles that

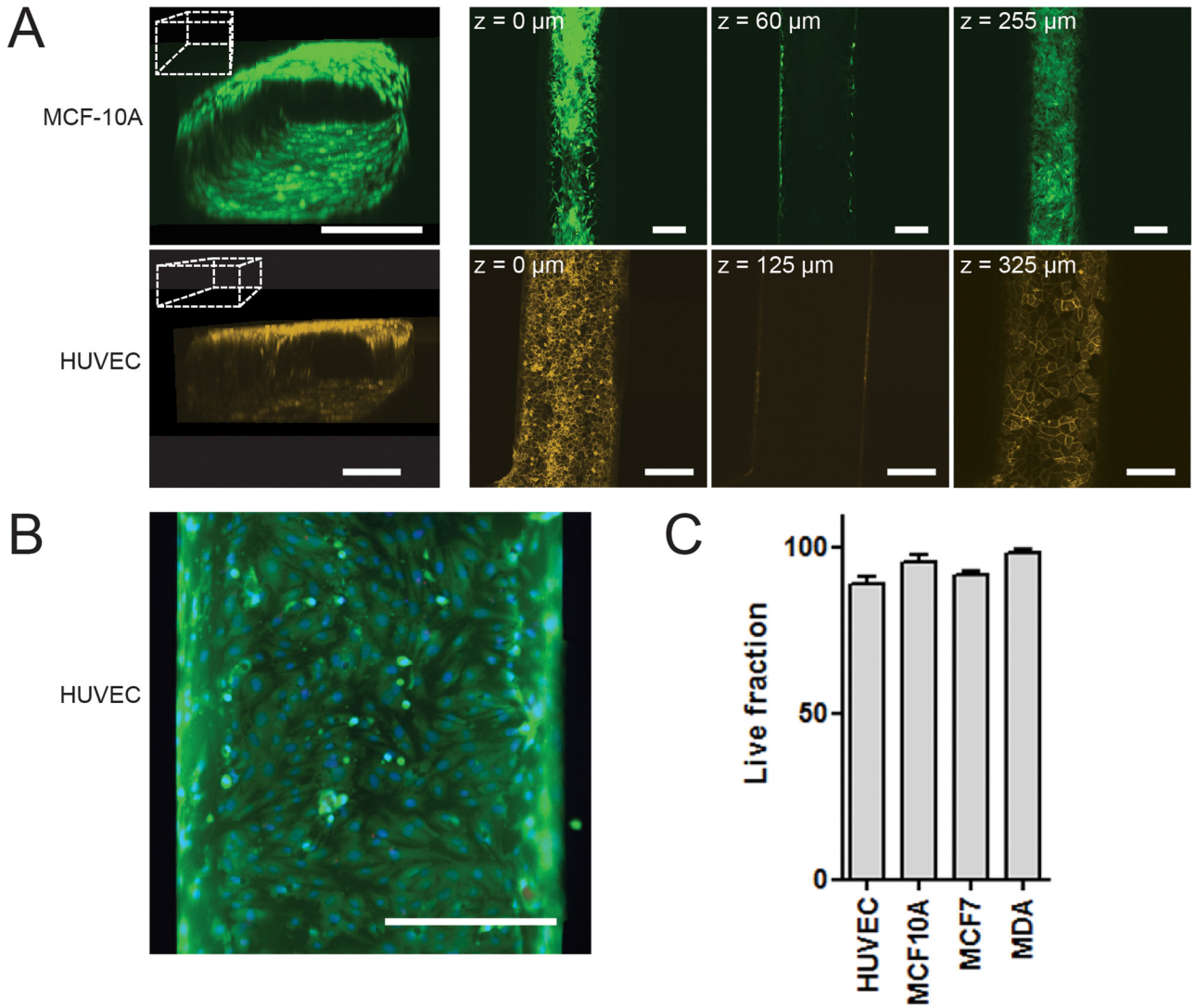

FIG. 2. Epithelial and endothelial-lined lumens. (a) MCF-10A cells (top row) were stained with CellTracker Green, and HUVECs (bottom row) were stained for CD31 after 24 h. 3D reconstructed confocal z-stack of MCF-10A and HUVEC lumens are shown (left) beside the confocal images at 3 different focal planes (right). Dotted boxes represent the orientation of 3D images. (b) Calcein AM (green) and ethidium homodimer (red) were used to stain live and dead cells, respectively (HUVECs shown). Nuclei stained with Hoechst. (c) Live fractions for the four different cell types indicating >85% viability at 48 h. All scale bars = 200 μm.

reached the HUVECs by diffusion. We qualitatively observed the minimal migration of MCF-10A [Fig. 3(a)] and MCF-7 [Fig. 3(b)] cells, and in contrast, observed significant migration of MDA-MB-231 [Fig. 3(c)] cells, as expected based on their invasive potential. To examine whether the MDA-MB-231 cells migrated due to its inherent invasiveness or due to the presence of HUVECs, we created parallel lumens consisting of MDA-MB-231s in both lumens [Fig. 3(d)], with the left lumen containing CellTracker Red MDA-MB-231s and the right lumen containing CellTracker Green MDA-MB-231s. We observed the migration of both red and green MDA-MB-231s into the migration port, but observed qualitatively that MDA-MB-231s migrated farther toward HUVECs than toward other MDA-MB-231 cells [Figs. 3(c) vs 3(d)].

To quantify these observations, we analyzed the fluorescence images and calculated various cell migration metrics within the migration ports, including the number of migrated cells into each migration port (where a single migration port is considered one ROI) [Fig. 4(a)], the area covered by migrated cells in each ROI [Fig. 4(b)], and the horizontal distance traveled by individual migrated cells into the ROI [Fig. 4(c)]. In the case of number of migrated cells and area coverage, we considered each ROI as a single independent measurement, whereas in the case of distance

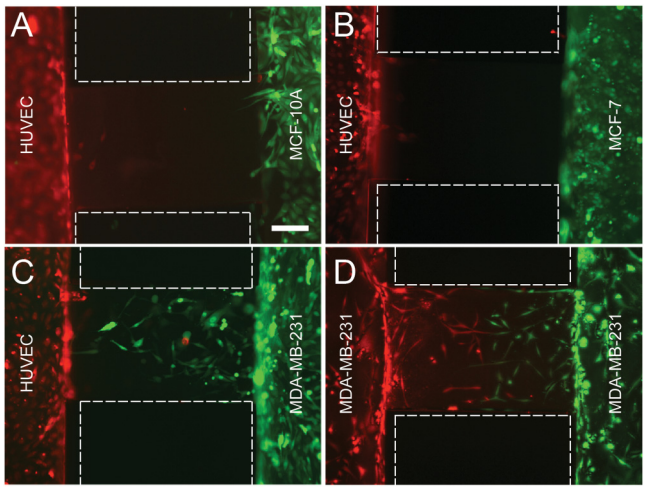

FIG. 3. Cell migration between parallel lumens. Images show representative regions of interest (ROIs) for a single migration port (1 of 3 parallel migration ports per system). CellTracker Red was used to stain cells loaded in the left lumen, and CellTracker Green was used to stain cells loaded in the right lumen. (a) HUVEC:MCF-10A coculture, (b) HUVEC:MCF-7 coculture, and (c) HUVEC: MDA-MB-231 coculture. (d) MDA-MB-231 in both lumens. Scale bar = 200 μm.

traveled, we considered each cell as a single measurement. The data showed that across all three metrics, MDA-MB-231 cells migrated the most toward HUVECs, and above its intrinsic migratory behavior in monoculture with MDA-MB-231 cells in both microchannels [Figs. 4(d)–4(f)]. MDA-MB-231 cells intrinsically migrated in higher numbers, covering larger areas, and over longer distances compared to both MCF-7s and MCF-10As in coculture with HUVECs, while MCF-10A cells tended to migrate over longer distances compared to MCF-7 cells, even though the number of migrated cells and area covered appeared to be similar [Figs. 4(d)–4(f)].

Migration of endothelial cells in chemotactic gradient

Our observations of epithelial cell migration between parallel lumens—and lack of concurrent endothelial cell migration—led us to investigate the potential reasons affecting the motility of endothelial cells in our cocultures. Because we expected some endothelial migration as a chemotactic response to the soluble factors secreted by mammary epithelial cells in a luminal structure, we were interested in demonstrating such chemotaxis of endothelial cells in our device, both to establish the baseline gradient necessary to induce chemotaxis and to establish the versatility of the platform to be used for chemical gradients and an angiogenesis assay. Thus, we created HUVEC lumens in the left microchannel as previously described and added vascular endothelial growth factor (VEGF) in the parallel right microchannel in varying concentrations to serve as the chemotactic source. 24 h after VEGF addition, serum-starved HUVEC cells migrated toward the VEGF source in a concentration-dependent manner [Fig. 5(a)]. Note that serum starvation ensured that the migration was due to the VEGF gradient and not due to other serum-derived growth factors. Indeed, serum-starved HUVECs responded to serum, as 2% FBS in the medium filling the right channel (RC) was sufficient to induce endothelial cell migration. In addition, we quantified HUVEC migration using the three migration metrics described previously and found that HUVECs migrated in a concentration-dependent manner toward the VEGF source or serum within 24 h [Figs. 5(b)–5(d)].

Based on these results, we sought to understand in more detail the biomolecular transport of VEGF over the entire 24-h time period. We performed numerical simulations in our 3D model over 24-h using COMSOL and studied the VEGF diffusion over time for a given starting VEGF concentration [e.g., 500 ng/ml starting VEGF concentration in Fig. 5(e)], and studied VEGF concentration profiles at 24 h for a range of different starting VEGF concentrations [Fig. 5(f)]. A VEGF concentration of 500 ng/ml was chosen to represent the experimental condition tested that led to the highest motility observed.

DISCUSSION

The rationale for developing our microfluidic coculture system with parallel lumens was to recapitulate the 3D luminal structures of neighboring mammary ducts and blood vessels of the mammary gland microenvironment [Fig. 1(f)] and to create an advanced *in vitro* model for studying epithelial and endothelial crosstalk in a breast cancer context. The lumens were created using a simple method adapted from a previously described viscous finger patterning technique,[30] enabling us to incorporate into our model both dimensionality and cell-matrix interactions that are often not captured by other standard 2D models,[39] and some microfluidic models. Although the importance of employing 3D rather than 2D culture models is generally well established,[13,40,41] there is increasing evidence that 3D lumens—particularly for endothelial and epithelial cells—behave and respond differently than their 2D monolayer counterparts. Bischel and co-workers reviewed and built on evidence supporting the importance of a 3D lumen by performing side-by-side 2D vs 3D cultures of various endothelial cells (HUVECs, induced pluripotent stem cell-derived ECs), and discovered that secretory profiles between 2D and 3D cultures of the same cell type were completely distinct.[42] More recently, patient-specific tumor and normal ECs were cultured in 2D and 3D formats, and it was also discovered that various proangiogenic secreted factors—including vascular endothelial growth factor A (VEGFA)—were differentially expressed and secreted by the 3D lumen cultures compared to the other formats.[43] For this reason, our group has continued to incorporate 3D luminal structures in our biomicrofluidic devices for both vascular and cancer studies.[44,45] We expect that our 3D lumens are also behaving distinctly from 2D HUVEC monolayers, although a side-by-side comparison is needed to show that these differences lead to distinct responses in cancer cell migration.

We showed here how both endothelial and epithelial confluent monolayers can be formed and can remain viable, with prominent cell-cell contacts in the case of the endothelial lining. Improvement in cell viability was attributed to the addition of medium-filled reservoirs at the outlet ports, which reduced the need for frequent medium replenishments in our static setup. Future advances of this system may involve adding perfusion and shear flow over the endothelium to mimic mechanobiological cues[46] as well as the addition

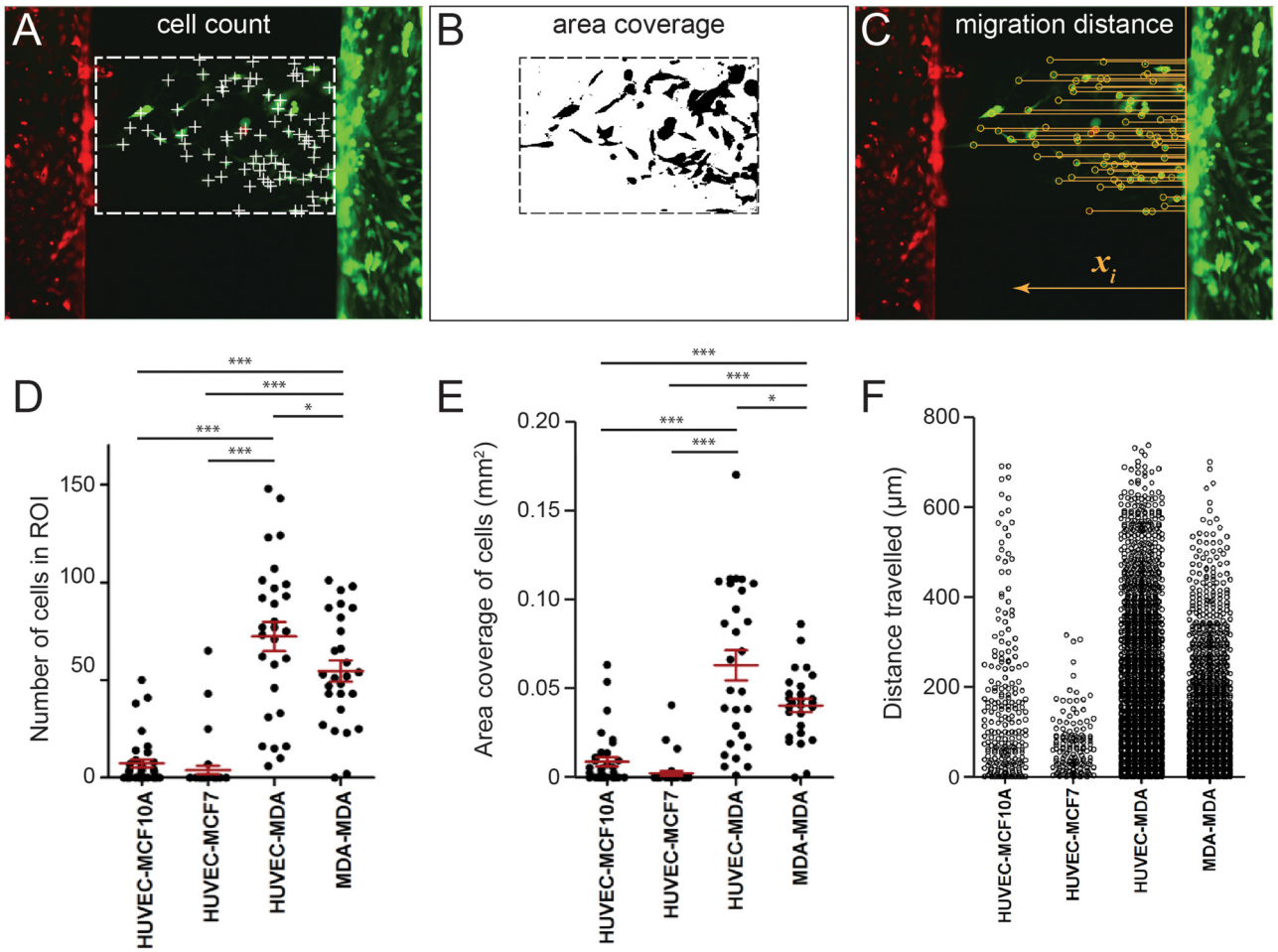

FIG. 4. Quantification of epithelial cell migration between parallel lumens. (a) Number of migrated cells (marked as white "+") was determined in each migration port (or ROI) using the ImageJ Find Maxima function. (b) Area covered by migrated cells in each ROI was determined in each migration port using the ImageJ Analyze Particles function. (c) Distance traveled by individual migrated cells (cell marked as yellow "o" and distance marked as yellow line) was determined by extracting the *x*-value from the list of *x*-*y* coordinates of all migrated cells in the ROI. The illustration shows x_i values as straight yellow lines from the edge of the right lumen into the migration port. (d) Graph of number of migrated cells within a single migration port vs culture type. (e) Graph of area coverage by migrated cells within a single migration port vs culture type. (f) Travel distances of individual migrated cells within a single migration port, compiled from all experiments ($n = 6$). ***$p < 0.0001$ and *$p < 0.05$.

of an outer layer of myoepithelial cells surrounding the inner luminal epithelial cells [Fig. 1(f)] to form a more accurate representation of the mammary acinar architecture.[15,47]

One of the main reasons for developing our parallel lumen model was to investigate the potential for concomitant migration of epithelial cells (toward an endothelial lumen) and endothelial cells (toward an epithelial lumen). Crosstalk between epithelial and endothelial cells has been well characterized,[9,48,49] and the onset of angiogenesis under premalignant conditions has also been recognized.[6,50,51] We thus hypothesized that endothelial-epithelial crosstalk in a 3D luminal context would generate soluble factor gradients in both directions, potentially driving migration of both cell types into the region between the parallel lumens. Interestingly, for all three coculture setups (involving HUVECs cocultured with one of the mammary epithelial cell lines), we observed only epithelial cell migration—most prominently by the MDA-MB-231 cell line—and no endothelial cell migration at all. In terms of the MDA-MB-231 cell line, these cells are known to possess inherent motility greater than that of MCF-7 and MCF-10A cells due to their metastatic potential.[52] Our results confirmed these differences between cell lines. First, MDA-MB-231 cells in monoculture (in both lumens) had higher migration profiles than both MCF-7 and MCF-10A cells in coculture with HUVECs. Second, MDA-MB-231 cells in coculture with HUVECs showed an even higher migration profile than MDA-MB-231 cells in monoculture [Figs. 4(d)–4(f)], suggesting that HUVECs further enhanced MDA-MB-231 migration above their baseline levels, perhaps via secretory chemokines such as CXCL12 and epidermal growth factor (EGF)[53,54] that are

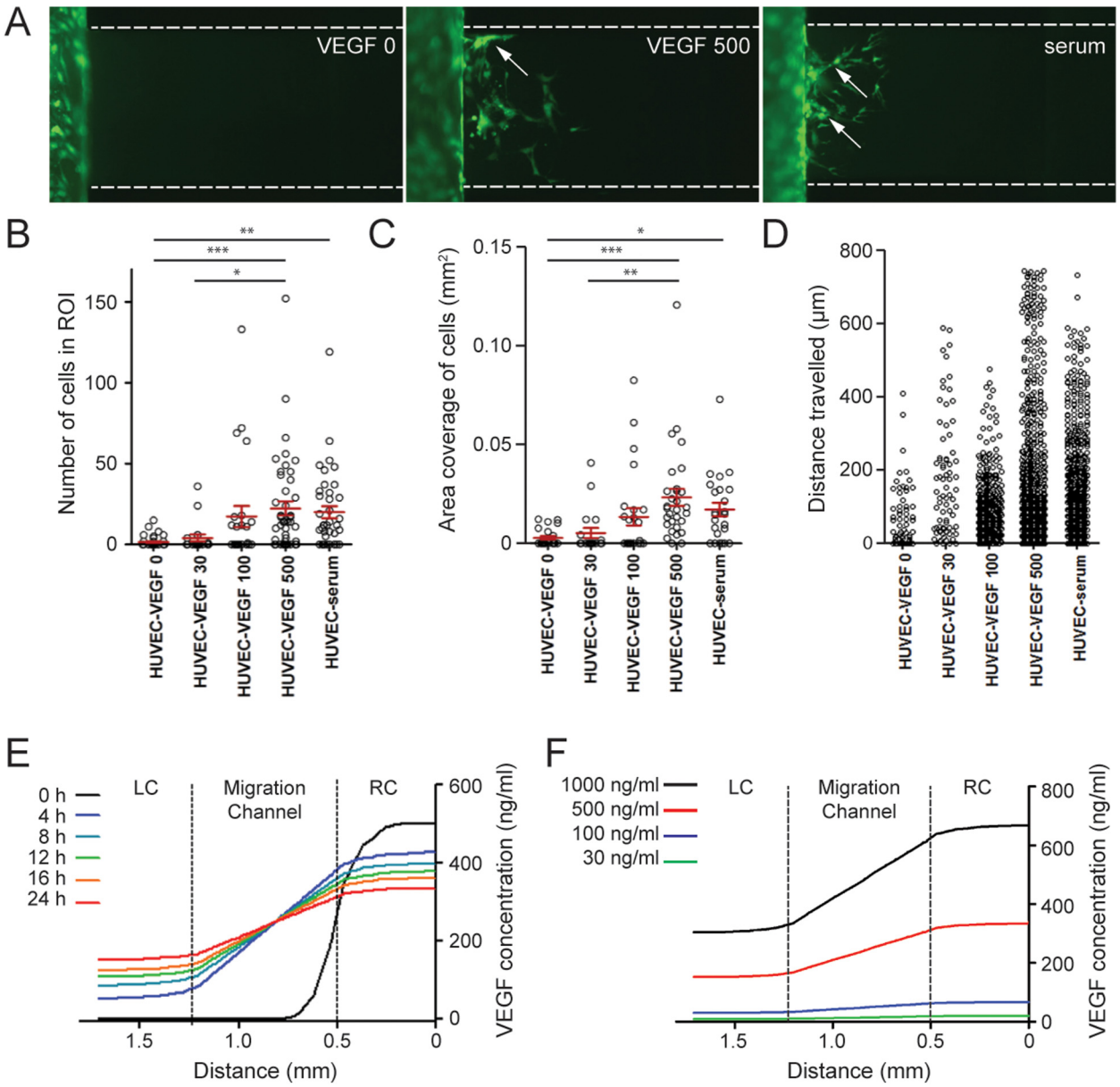

FIG. 5. Endothelial cell migration induced by VEGF gradient. (a) HUVECs in the left lumen were prestained with CellTracker Green to track cell migration toward the right lumen, which contained either a VEGF source or serum. Three representative images are shown, including serum-free media (VEGF 0), 500 ng/ml VEGF, and serum-containing medium (serum). (b) Graph of number of migrated cells within a single migration port vs VEGF concentration. (c) Graph of area coverage by migrated cells within a single migration port vs VEGF concentration. (d) Travel distances of individual migrated cells within a single migration port vs VEGF concentration, compiled from all experiments ($n = 8$). (e)–(f) COMSOL simulations of VEGF concentration profiles in the migration port showing (e) the case of 500 ng/ml starting VEGF concentration in the right channel (RC) at different timepoints, and (f) for $t = 24$ h for different starting VEGF concentrations in the RC. Note that the red curve in both graphs represents the same case, i.e., 24-h at 500 ng/ml starting VEGF concentration. ***$p < 0.0001$, **$p < 0.01$, and *$p < 0.05$.

known to promote MDA-MB-231 invasion.[55] Taken together, MCF-7 and MCF-10A cell lines must, therefore, possess low baseline migration profiles with minimal enhancement from HUVECs, whereas the MDA-MB-231 cell line possesses a high baseline migration profile that is further enhanced by endothelial crosstalk. These results were enabled by our microfluidic parallel lumen system and highlight the need and importance of coculturing multiple cell types to recapitulate the tissue microenvironment.[56–59]

Our findings that HUVECs did not migrate in any of the coculture setups led us to investigate the potential reasons for this lack of motility. We modified our parallel lumen system by replacing the epithelial lumen with a cell-free lumen loaded with VEGF. The presence of hydrogel in the migration ports allowed controlled VEGF diffusion into the migration ports and permitted a sustained gradient for 24 h. We observed a migratory response of HUVECs to VEGF in a concentration-dependent manner, with a moderate migration profile at a 100-ng/ml starting VEGF concentration, and a higher migration profile at a 500-ng/ml starting VEGF concentration. In these experiments, serum starvation of HUVECs was found to be critical for the migratory response. As can be seen from the results, the presence of 2% FBS in the medium in the right microchannel was sufficient to induce endothelial cell migration even without VEGF (Fig. 5).

Our observations showed that HUVECs migrated as expected in our microfluidic system in the presence of a chemotactic VEGF gradient, and that the lack of migration in coculture with epithelial cells may be due to an insufficient VEGF concentration and VEGF gradient to induce migration. Our numerical simulations predicted that after 24 h, the edge of the left lumen (proximal to the migration port) was exposed to ~200 ng/ml VEGF if the right lumen started at 500 ng/ml VEGF, and that this location was exposed to <50 ng/ml VEGF if the right lumen started at 100 ng/ml VEGF. These values are consistent with previous reports regarding VEGF concentrations needed to induce HUVEC migration.[60,61] We note that most of the migration was observed to occur after only 16 h had elapsed, suggesting the left lumen was exposed to slightly lower VEGF concentrations than those stated above, but we report these values to represent those at our 24-h endpoints. Experiments could be designed to further test VEGF-induced migration by shortening the migration ports to create a steeper gradient while maintaining the same starting VEGF concentration or by introducing perfusion to maintain a constant VEGF source.

In terms of endothelial morphology, HUVECs that migrated into the migration ports in the presence of a VEGF gradient appeared to exhibit morphology similar to an angiogenic sprout [Fig. 5(a), white arrows]. This was an interesting observation and will require further examination. Nevertheless, our microfluidic parallel lumen system showed the versatility to be potentially used as an angiogenesis model comparable to other microfluidic angiogenesis systems.[23,24,30,62–66]

Regarding data analyses, it was evident from our measurements of the three migration metrics (i.e., number of migrated cells, area coverage by migrated cells, and distance traveled by individual migrating cells) that our experiments had significant variability. We conducted 6 independent experiments for each coculture type and 8 independent experiments for the VEGF gradient experiments, and we noticed variability between experiments, between systems within the same experiment, and even between ROIs within the same system (i.e., sometimes cells migrated evenly in all three migration ports, while other times the cells migrated in only one of the three migration ports). Faced with such variability, we decided that presenting all the data as individual measurements (i.e., individual ROIs for total cell numbers and area coverage and individual cells for travel distance) preserved data granularity, and in this manner, trends in the data were captured. In some cases, a data point within our dataset that is typically considered to be an outlier (i.e., a significantly higher number of migrated cells in one ROI) was found to be an example of a higher tendency to migrate, given that an increase in frequency of such outliers was often observed across the entire set of experiments. As a convenience to readers, we reported conventional *p*-values where possible, recognizing their limitations particularly for this dataset.[67]

We envision that this microfluidic parallel lumen system can be applied to study outstanding questions in breast cancer tumor development, specifically regarding aspects of endothelial-epithelial crosstalk, cell migration, and angiogenesis. The system can be further adapted to incorporate perfusion and shear flow on the endothelium and can be extended toward longer-term studies to examine angiogenic sprouting, vessel maturation, epithelial-mesenchymal transition (EMT), and tumor cell intravasation, all in a 3D luminal context that more closely resembles the architecture in the human mammary gland. Furthermore, the platform may be used to test drug candidates for inhibition of angiogenesis and tumor cell invasion, especially given its arrayable and scalable format, and its compatibility with automated liquid handling strategies.

CONCLUSIONS

We have developed and applied a microfluidic coculture system consisting of parallel lumens to model key elements of the mammary gland microenvironment for the purpose of advancing breast cancer research. The parallel lumen model allowed us to establish 3D luminal structures for both endothelial and epithelial cell layers, enabling the study of the concurrent migration of epithelial and endothelial cells in a crosstalk environment. We created lumens using several different epithelial cell lines and established migration profiles for each cell line based on number of migrated cells, area coverage by migrated cells, and distance traveled by individual migrating cells. Our analyses at the single-cell level enabled the observation of trends that revealed additional insights regarding cell behavior, which was further corroborated by numerical modeling of VEGF gradients within our system. This microfluidic coculture system with parallel lumens has potential for future applications in studying endothelial-epithelial crosstalk in the context of breast cancer and may be used for functional screening in the drug development process.

ACKNOWLEDGMENTS

E.W.K.Y. acknowledges financial support from the Canada Foundation for Innovation (CFI) John R Evans Leadership Fund (No. 32171), the Natural Sciences and Engineering Research Council of Canada (NSERC) Discovery (Grant No. 436117-2013), the Canadian Cancer Society Research Institute (CCSRI) Innovation (Grant No. 702525), the Early Researcher Award from Ontario Ministry of Research and Innovation (No. ER15-11-058), and the Cancer Research Society (CRS, No. 20172).

REFERENCES

[1]T. Vargo-Gogola and J. M. Rosen, "Modelling breast cancer: One size does not fit all," Nat. Rev. Cancer **7**, 659–672 (2007).

[2]N. Reymond, B. B. D'Agua, and A. J. Ridley, "Crossing the endothelial barrier during metastasis," Nat. Rev. Cancer **13**, 858–870 (2013).
[3]C. M. Nelson and M. J. Bissell, "Of extracellular matrix, scaffolds, and signaling: Tissue architecture regulates development, homeostasis, and cancer," Annu. Rev. Cell Dev. Biol. **22**, 287–309 (2006).
[4]F. Hassiotou and D. Geddes, "Anatomy of the human mammary gland: Current status of knowledge," Clin. Anat. **26**, 29–48 (2013).
[5]M. de Palma, D. Biziato, and T. V. Petrova, "Microenvironmental regulation of tumour angiogenesis," Nat. Rev. Cancer **17**, 457–474 (2017).
[6]S. R. Menakuru, N. J. Brown, C. A. Staton, and M. W. R. Reed, "Angiogenesis in pre-malignant conditions," Br. J. Cancer **99**, 1961–1966 (2008).
[7]A. Thompson *et al.*, "Evaluation of the current knowledge limitations in breast cancer research: A gap analysis," Breast Cancer Res. **10**(R26), 1–25 (2008).
[8]B. Weigelt, C. M. Ghajar, and M. J. Bissell, "The need for complex 3D culture models to unravel novel pathways and identify accurate biomarkers in breast cancer," Adv. Drug Deliv. Rev. **69**, 42–51 (2014).
[9]M.-F. Pang *et al.*, "TGF-beta 1-induced EMT promotes targeted migration of breast cancer cells through the lymphatic system by the activation of CCR7/CCL21-mediated chemotaxis," Oncogene **35**, 748–760 (2016).
[10]G. V. Rodriguez, A. Abrahamsson, L. D. E. Jensen, and C. Dabrosin, "Estradiol promotes breast cancer cell migration via recruitment and activation of neutrophils," Cancer Immunol. Res. **5**, 234–247 (2017).
[11]E. Leung *et al.*, "Blood vessel endothelium-directed tumor cell streaming in breast tumors requires the HGF/C-Met signaling pathway," Oncogene **36**, 2680–2692 (2017).
[12]R. Auerbach, R. Lewis, B. Shinners, L. Kubai, and N. Akhtar, "Angiogenesis assays: A critical overview," Clin. Chem. **49**, 32–40 (2003).
[13]K. L. Schmeichel and M. J. Bissell, "Modeling tissue-specific signaling and organ function in three dimensions," J. Cell Sci. **116**, 2377–2388 (2003).
[14]C. M. Nelson, M. M. VanDuijn, J. L. Inman, D. A. Fletcher, and M. J. Bissell, "Tissue geometry determines sites of mammary branching morphogenesis in organotypic cultures," Science **314**, 298–300 (2006).
[15]L. Chanson *et al.*, "Self-organization is a dynamic and lineage-intrinsic property of mammary epithelial cells," Proc. Natl. Acad. Sci. U.S.A. **108**, 3264–3269 (2011).
[16]S. Swaminathan, O. Ngo, S. Basehore, and A. M. Clyne, "Vascular endothelial-breast epithelial cell coculture model created from 3D cell structures," ACS Biomater. Sci. Eng. **3**, 2999–3006 (2017).
[17]E. W. K. Young and D. J. Beebe, "Fundamentals of microfluidic cell culture in controlled microenvironments," Chem. Soc. Rev. **39**, 1036–1048 (2010).
[18]E. W. K. Young, "Cells, tissues, and organs on chips: Challenges and opportunities for the cancer tumor microenvironment," Integr. Biol. **5**, 1096–1109 (2013).
[19]C. Zheng *et al.*, "Quantitative study of the dynamic tumor–endothelial cell interactions through an integrated microfluidic coculture system," Anal. Chem. **84**, 2088–2093 (2012).
[20]I. K. Zervantonakis *et al.*, "Three-dimensional microfluidic model for tumor cell intravasation and endothelial barrier function," Proc. Natl. Acad. Sci. U.S.A. **109**, 13515–13520 (2012).
[21]R. Huang *et al.*, "Investigation of tumor cell behaviors on a vascular microenvironment-mimicking microfluidic chip," Sci. Rep. **5**, 17768 (2015).
[22]J. W. Song and L. L. Munn, "Fluid forces control endothelial sprouting," Proc. Natl. Acad. Sci. U.S.A. **108**, 15342–15347 (2011).
[23]J. W. Song, D. Bazou, and L. L. Munn, "Anastomosis of endothelial sprouts forms new vessels in a tissue analogue of angiogenesis," Integr. Biol. **4**, 857–862 (2012).
[24]A. B. Theberge *et al.*, "Microfluidic multiculture assay to analyze biomolecular signaling in angiogenesis," Anal. Chem. **87**, 3239–3246 (2015).
[25]E. W. K. Young and C. A. Simmons, "Macro- and microscale fluid flow systems for endothelial cell biology," Lab Chip **10**, 143–160 (2010).
[26]K. H. K. K. Wong, J. M. Chan, R. D. Kamm, and J. Tien, "Microfluidic models of vascular functions," Annu. Rev. Biomed. Eng. **14**, 205–230 (2012).
[27]E. W. K. Young, "Advances in microfluidic cell culture systems for studying angiogenesis," J. Lab. Autom. **18**, 427–436 (2013).
[28]E. Um, J. M. Oh, S. Granick, and Y.-K. Cho, "Cell migration in microengineered tumor environments," Lab Chip **17**, 4171–4185 (2017).
[29]S. Even-Ram and K. M. Yamada, "Cell migration in 3D matrix," Curr. Opin. Cell Biol. **17**, 524–532 (2005).
[30]L. L. Bischel, E. W. K. Young, B. B. R. Mader, and D. J. Beebe, "Tubeless microfluidic angiogenesis assay with three-dimensional endothelial-lined microvessels," Biomaterials **34**, 1471–1477 (2013).
[31]L. L. Bischel, D. J. Beebe, and K. E. Sung, "Microfluidic model of ductal carcinoma in situ with 3D, organotypic structure," BMC Cancer **15**, 12 (2015).
[32]V. K. Lee *et al.*, "Generation of multi-scale vascular network system within 3D hydrogel using 3D bio-printing technology," Cell. Mol. Bioeng. **7**, 460–472 (2014).
[33]E. Berthier and D. J. Beebe, "Flow rate analysis of a surface tension driven passive micropump," Lab Chip **7**, 1475–1478 (2007).
[34]N. Kuzmic, T. Moore, D. Devadas, and E. W. K. Young, "Modelling of endothelial cell migration and angiogenesis in microfluidic cell culture systems," Biomech. Model. Mechanobiol. **18**, 717–731 (2019).
[35]G. Whitesides, E. Ostuni, S. Takayama, X. Jiang, and D. Ingber, "Soft lithography in biology and biochemistry," Annu. Rev. Biomed. Eng. **3**, 335–373 (2001).
[36]E. W. K. Young *et al.*, "Microscale functional cytomics for studying hematologic cancers," Blood **119**, E76–E85 (2012).
[37]N. V. Menon, H. M. Tay, S. N. Wee, K. H. H. Li, and H. W. Hou, "Micro-engineered perfusable 3D vasculatures for cardiovascular diseases," Lab Chip **17**, 2960–2968 (2017).
[38]S. J. Trietsch *et al.*, "Membrane-free culture and real-time barrier integrity assessment of perfused intestinal epithelium tubes," Nat. Commun. **8**, 262 (2017).
[39]L. L. Bischel *et al.*, "A microfluidic coculture and multiphoton FAD analysis assay provides insight into the influence of the bone microenvironment on prostate cancer cells," Integr. Biol. **6**, 627–635 (2014).
[40]B. M. Baker and C. S. Chen, "Deconstructing the third dimension—How 3D culture microenvironments alter cellular cues," J. Cell Sci. **125**, 3015–3024 (2012).
[41]K. Duval *et al.*, "Modeling physiological events in 2D vs. 3D cell culture," Physiology **32**, 266–277 (2017).
[42]L. L. Bischel *et al.*, "The importance of being a lumen," FASEB J. **28**, 4583–4590 (2014).
[43]J. A. Jimenez-Torres *et al.*, "Patient-specific organotypic blood vessels as an in vitro model for anti-angiogenic drug response testing in renal cell carcinoma," EBioMedicine **42**, 408–419 (2019).
[44]X. Mei *et al.*, "Microfluidic platform for studying osteocyte mechanoregulation of breast cancer bone metastasis," Integr. Biol. **11**, 119–129 (2019).
[45]J. F. Wong, M. D. Mohan, E. W. K. Young, and C. A. Simmons, "Integrated electrochemical measurement of endothelial permeability in a 3D hydrogel-based microfluidic vascular model," Biosens. Bioelectron. **147**, 111757 (2020).
[46]J. Shemesh, I. Jalilian, A. Shi, G. H. Yeoh, K. Tate, L. Melissa, and M. E. Warkian, "Flow-induced stress on adherent cells in microfluidic devices," Lab Chip **15**, 4114–4127 (2015).
[47]J. J. Campbell, N. Davidenko, M. M. Caffarel, R. E. Cameron, and C. J. Watson, "A multifunctional 3D Co-culture system for studies of mammary tissue morphogenesis and stem cell biology," PLoS One **6**, e25661 (2011).
[48]J. A. Burger and T. J. Kipps, "CXCR4: A key receptor in the crosstalk between tumor cells and their microenvironment," Blood **107**, 1761–1767 (2006).
[49]C. F. Buchanan *et al.*, "Cross-talk between endothelial and breast cancer cells regulates reciprocal expression of angiogenic factors in vitro," J. Cell. Biochem. **113**, 1142–1151 (2012).
[50]J. E. Bluff *et al.*, "Angiogenesis is associated with the onset of hyperplasia in human ductal breast disease," Br. J. Cancer **101**, 666–672 (2009).
[51]M. Raica, A. M. Cimpean, and D. Ribatti, "Angiogenesis in pre-malignant conditions," Eur. J. Cancer **45**, 1924–1934 (2009).
[52]E. Walker-Nasir, J. F. Codington, M. R. Jahnke, T. Fuller, and R. W. Jeanloz, "Isolation and partial characterization of surface components of cell line MDA-MB-231 derived from a human metastatic breast carcinoma," J. Natl. Cancer Inst. **69**, 371–380 (1982).

[53]L. A. Pitt, A. N. Tikhonova, H. Hu, T. Trimarchi, B. King, Y. Gong, M. Sanchez-Martin, A. Tsirigos, D. R. Littman, A. Ferrando, S. J. Morrison, D. R. Fooksman, I. Aifantis, and S. R. Schwab, "CXCL12-producing vascular endothelial niches control acute T cell leukemia maintenance," Cancer Cell **27**, 755–768 (2015).
[54]Z. Zhang, Z. Dong, I. S. Lauxen, M. S. A. Filho, and J. E. Nör, "Endothelial cell-secreted EGF induces epithelial to mesenchymal transition and endows head and neck cancer cells with stem-like phenotype," Cancer Res. **74**, 2869–2881 (2014).
[55]B. Mosadegh, W. S. Shur-Jen, W. Noo, and L. Jeon, "Epidermal growth factor promotes breast cancer cell chemotaxis in CXCL12 gradients," Biotechnol. Bioeng. **100**, 105–113 (2008).
[56]M. C. Regier *et al.*, "Transitions from mono- to co- to tri-culture uniquely affect gene expression in breast cancer, stromal, and immune compartments," Biomed. Microdevices **18**, 70 (2016).
[57]C. Pak *et al.*, "Microc3: An ex vivo microfluidic cis-coculture assay to test chemosensitivity and resistance of patient multiple myeloma cells," Integr. Biol. **7**, 643–654 (2015).
[58]Z. Zhang *et al.*, "Expansion of CTCs from early stage lung cancer patients using a microfluidic co-culture model," Oncotarget **5**, 12383–12397 (2014).
[59]J. S. Jeon *et al.*, "Generation of 3D functional microvascular networks with human mesenchymal stem cells in microfluidic systems," Integr. Biol. **6**, 555–563 (2014).
[60]D. Stone, M. Phaneuf, N. Sivamurthy, and W. C. Quist, "A biologically active VEGF construct in vitro: Implications for bioengineering-improved prosthetic vascular grafts," J. Biomed. Mater. Res. **59**, 160–165 (2002).
[61]M. McMullen, R. Keller, M. Sussman, and K. Pumiglia, "Vascular endothelial growth factor-mediated activation of p38 is dependent upon Src and RAFTK/Pyk2," Oncogene **23**, 1275–1282 (2004).
[62]C. Kim, J. Kasuyaa, J. Jeon, S. Chung, and R. D. Kamm, "A quantitative microfluidic angiogenesis screen for studying anti-angiogenic therapeutic assay," Lab Chip **15**, 301–310 (2015).
[63]S. S. Verbridge *et al.*, "Physicochemical regulation of endothelial sprouting in a 3D microfluidic angiogenesis model," J. Biomed. Mater. Res. A **101**, 2948–2956 (2013).
[64]H. Lee, W. Park, H. Ryu, and N. L. Jeon, "A microfluidic platform for quantitative analysis of cancer angiogenesis and intravasation," Biomicrofluidics **8**, 054102 (2014).
[65]D.-H. T. Nguyen *et al.*, "Biomimetic model to reconstitute angiogenic sprouting morphogenesis in vitro," Proc. Natl. Acad. Sci. U.S.A. **110**, 6712–6717 (2013).
[66]S. Chen *et al.*, "A perforated microhole-based microfluidic device for improving sprouting angiogenesis in vitro," Biomicrofluidics **11**, 054111 (2017).
[67]R. L. Wasserstein and N. A. Lazar, "The ASA's statement on p-values: Context, process, and purpose," Am. Stat. **70**, 129–131 (2016).